The Astrophysical Journal, 651:401–407, 2006 November 1

FURTHER EVIDENCE FOR VARIABLE SYNCHROTRON EMISSION IN XTE J1118+480 IN OUTBURST

R. I. Hynes,[1,2] E. L. Robinson,[3] K. J. Pearson,[1,2] D. M. Gelino,[2,4] W. Cui,[5] Y. Q. Xue,[5] M. A. Wood,[6] T. K. Watson,[7] D. E. Winget,[3] and I. M. Silver[6]

Received 2005 November 15; accepted 2006 July 11

ABSTRACT

We present simultaneous multicolor infrared and optical photometry of the black hole X-ray transient XTE J1118+480 during its short 2005 January outburst, supported by simultaneous X-ray observations. The variability is dominated by short timescales, ~10 s, although a weak superhump also appears to be present in the optical. The optical rapid variations, at least, are well correlated with those in X-rays. Infrared JHK_s photometry, as in the previous outburst, exhibits especially large-amplitude variability. The spectral energy distribution (SED) of the variable infrared component can be fitted with a power law of slope $\alpha = -0.78 \pm 0.07$, where $F_\nu \propto \nu^\alpha$. There is no compelling evidence for evolution in the slope over five nights, during which time the source brightness decayed along almost the same track as seen in variations within the nights. We conclude that both short-term variability and longer timescale fading are dominated by a single component of constant spectral shape. We cannot fit the SED of the IR variability with a credible thermal component, either optically thick or thin. This IR SED is, however, approximately consistent with optically thin synchrotron emission from a jet. These observations therefore provide indirect evidence to support jet-dominated models for XTE J1118+480 and also provide a direct measurement of the slope of the optically thin emission, which is impossible, based on the average spectral energy distribution alone.

Subject headings: accretion, accretion disks — binaries: close — stars: individual (XTE J1118+480)

1. INTRODUCTION

The black hole X-ray transient (BHXRT) XTE J1118+480 has proven to be a crucial object for understanding the class. It is one of the best objects for multiwavelength study, as it suffers an exceptionally low interstellar extinction, allowing broadband observations encompassing even the extreme-UV region (Hynes et al. 2000; McClintock et al. 2001; Chaty et al. 2003). It also stands out in possessing the shortest period yet known among objects with black hole primaries (4.1 hr) and has exhibited only low-luminosity hard-state outbursts, reaching just 1.2×10^{36} ergs s^{-1} (McClintock et al. 2001).

The increasingly dominant paradigm for understanding the emission from XTE J1118+480, and from hard-state BHXRTs in general, is that it (usually) involves an evaporated hot inner disk launching a compact jet (Markoff et al. 2001; Yuan et al. 2005). The jet is responsible for not only radio emission, but also much of the IR, optical, and possibly even some UV emission. The properties of the unusual UV, optical, and IR (UVOIR) variability also point to synchrotron emission rather than reprocessing of X-rays by a disk (Kanbach et al. 2001; Hynes et al. 2003). In fact it has even been proposed that the X-ray emission seen in the hard state could arise from synchrotron emission (Markoff et al. 2001), although this is not widely accepted and may be overwhelmed by a larger Comptonized X-ray component (Yuan et al. 2005).

Part of the difficulty in bridging from the UVOIR region to X-rays is that the former is likely a mixture of jet and disk emission, with the disk emission masking the break from flat-spectrum to optically thin synchrotron emission. Consequently, the position of the break and slope of the optically thin component are not directly observable, increasing the uncertainty in extrapolating to X-rays. The variability may provide the key to disentangling these components. To test this possibility, we have assembled serendipitous multiwavelength observations of XTE J1118+480 during the 2005 January outburst. The 2005 outburst was a much shorter and somewhat weaker event than that seen in 2000. It was discovered optically by Zurita et al. (2005a), with the first high points seen on 2005 January 9. The outburst was also detected at X-ray and radio wavelengths (Remillard et al. 2005; Pooley 2005; Rupen et al. 2005). The outburst faded rapidly, reaching near quiescence by late February (Zurita et al. 2005b). For a discussion of the outburst properties and long-term light curves, see Zurita et al. (2006).

2. OBSERVATIONS

2.1. *SARA* 0.9 m *Optical Observations*

XTE J1118+480 was observed using the SARA 0.9 m telescope located at Kitt Peak National Observatory. Observations used an Apogee AP7p CCD camera with an *R* filter. Exposure times were 10 s, with approximately 7 s intervening dead time. The raw data frames were bias-, dark-, and flat-field–corrected using standard IRAF routines. Once the data frames were calibrated, we extracted time series aperture photometry using the external IRAF package CCD_HSP, written by Antonio Kanaan (U. Federal Santa Catarina, Brazil). CCD_HSP automates the field alignment and photometry extraction for time series CCD data.

[1] Department of Physics and Astronomy, Louisiana State University, Baton Rouge, LA 70803; rih@phys.lsu.edu.

[2] Visiting Astronomer, Kitt Peak National Observatory, National Optical Astronomy Observatory, which is operated by the Association of Universities for Research in Astronomy, Inc. (AURA), under cooperative agreement with the National Science Foundation.

[3] McDonald Observatory and Department of Astronomy, University of Texas at Austin, 1 University Station C1400, Austin, TX 78712.

[4] Michelson Science Center, California Institute of Technology, Mail Stop 100-22, Pasadena, CA 91125.

[5] Department of Physics, Purdue University, 525 Western Avenue, West Lafayette, IN 47907.

[6] Department of Physics and Space Sciences, and SARA Observatory, Florida Institute of Technology, Melbourne, FL 32901.

[7] Southwestern University, 1001 East University Avenue, Georgetown, TX 78626.

TABLE 1
Log of Optical/IR Observations

Telescope and Instrument	UT Date and Time	Exposure (s)
SARA 0.9 m, AP7p	2005 Jan 13 06:03:04–13:50:50	10
	2005 Jan 15 06:02:57–13:53:07	10
McDonald 2.1 m, Argos	2005 Jan 13 07:42:07–09:04:39	1
McDonald 2.7 m, White Guider	2005 Jan 16 07:51:06–12:28:23	3
	2005 Jan 19 09:17:12–10:56:48	3
KPNO 2.1 m, SQIID	2005 Jan 15 09:59:49–14:00:29	2
	2005 Jan 16 08:01:48–13:52:09	2
	2005 Jan 17 10:28:01–13:51:59	1
	2005 Jan 18 07:54:30–13:54:12	2
	2005 Jan 19 09:39:40–13:53:08	2

2.2. *McDonald Observatory* 2.1 m *Optical Observations*

XTE J1118+480 was also observed using the Argos fast CCD camera (Nather & Mukadam 2004) on the McDonald Observatory 2.1 m telescope. About 1.5 hr of data were obtained in unfiltered white light. The data were taken as a continuous sequence of 1 s images with negligible intervening dead time. Conditions were mostly nonphotometric with 1″–2″ seeing, so differential photometry was performed relative to the same comparison star used in the IR. Data reduction employed a combination of IRAF routines to generate calibration files and then a custom IDL pipeline to apply calibrations and extract photometry. Bias structure and dark current were subtracted using many dark exposures of the same duration as the object frames. Residual time-dependent bias variations were removed using two partial bad columns, which are not light sensitive. Unfortunately, no flat fields were obtained in the unfiltered mode, so no sensitivity corrections were applied. Photometry was extracted using standard aperture photometry techniques.

2.3. *McDonald Observatory* 2.7 m *Optical Observations*

Additional optical observations of XTE J1118+480 were performed using the White Guider CCD camera on the McDonald Observatory 2.7 m telescope. The data were taken as a continuous sequence of 3 s *R*-band images with about 2 s of intervening dead time. Conditions appeared near photometric with 1″–2″ seeing, so absolute photometry was performed to maximize the signal-to-noise ratio. Conditions deteriorated toward the end of the January 19 run, so these data were discarded. This approach was necessary, as the comparison star used with Argos was not available with this instrument, and the brightest other comparison in the field was nearly 6 mag fainter than XTE J1118+480 in outburst. Initial data reduction used standard IRAF procedures to remove bias and flat-field the data. Aperture photometry of XTE J1118+480 used a 5″ aperture to minimize aperture losses.

2.4. *Kitt Peak National Observatory* 2.1 m *Infrared Observations*

Infrared photometry of XTE J1118+480 was obtained using the Simultaneous Quad Infrared Imaging Device (SQIID) on the 2.1 m telescope at the Kitt Peak National Observatory. Details are given in Tables 1 and 2. The camera records *J*, *H*, K_s, and *L* images simultaneously, although we found that the *L* data were of insufficient quality to be useful. JHK_s data were all of good quality, however, and obtained simultaneously with 1 s or 2 s exposures separated by ∼54 s of dead time. The image was nodded back and forth on alternating exposures to facilitate sky subtraction. The seeing was typically better than 1.″3 in *J*. Data reduction employed a combination of IRAF[8] routines to generate calibration files and then a custom IDL pipeline to apply calibrations and extract photometry.

Where possible, sky subtraction was performed by subtracting the average of immediately preceding and immediately following images. Sensitivity variations were corrected using an average of many sky flat images taken at twilight. We verified that these images acceptably flattened the sky background of target images before sky subtraction. Count rates were low enough that nonlinearity was below 1%, so no correction was applied.

Because of the source brightness during outburst, only one usable comparison star was present in the field, and this was fainter than our target. We therefore used the comparison star only as a check of the photometric stability and did not perform differential photometry. Fortunately, conditions were mostly photometric, at least sufficiently so that transparency variations are much smaller than the intrinsic variability of the target. The major

[8] IRAF is distributed by the National Optical Astronomy Observatory, which is operated by the Association of Universities for Research in Astronomy, Inc., under cooperative agreement with the National Science Foundation.

TABLE 2
Details of IR Photometry

UT Date	Total Number of Images	Good Images	Average Magnitude of XTE J1118+480		
			J	*H*	K_s
2005 Jan 15	221	205	12.92	12.49	11.97
2005 Jan 16	360	246	12.96	12.52	12.05
2005 Jan 17	210	147	13.03	12.64	12.10
2005 Jan 18	380	304	13.06	12.64	12.14
2005 Jan 19	270	257	13.10	12.70	12.19

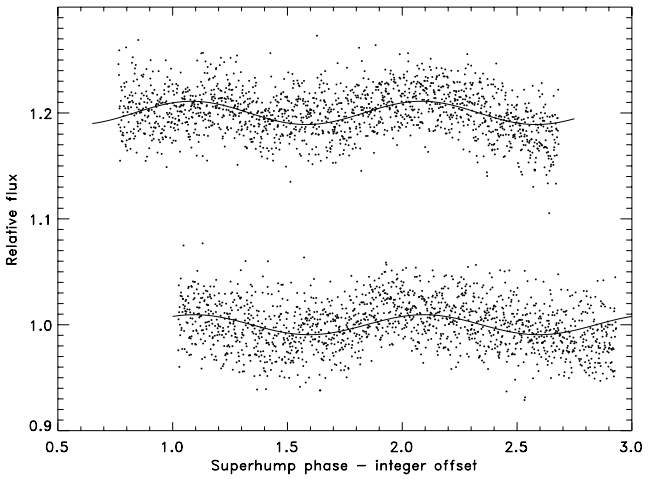

FIG. 1.—Modulation in SARA photometry folded on the preferred 1.0025 $P_{\rm orb}$ period, likely due to a superhump.

exception occurred at the end of the third night, so these points were not used.

Our absolute calibration is based on 2MASS photometry of the comparison star, 2MASS J11180724+4803527 (Cutri et al. 2003). This star has $J = 13.449 \pm 0.024$, $H = 12.825 \pm 0.028$, and $K_s = 12.610 \pm 0.022$, where the uncertainties are dominated by statistical effects and so should be uncorrelated. We checked this calibration against ARNICA standards AS 19-0 and AS 19-2 (Hunt et al. 1998) after transforming the latter in the 2MASS JHK_s system (Carpenter 2001). The standard yielded a consistent calibration, with comparable uncertainties, so we retained the 2MASS calibration for this work. Our average calibrated magnitudes for the target for each night are summarized in Table 2. The calibrated magnitudes were converted to fluxes according to Cutri et al. (2003). After folding in uncertainties in conversion from magnitudes to fluxes, we estimate that the systematic uncertainties in our calibrated fluxes are then 2.8% in J, 3.2% in H, and 2.8% in K_s.

2.5. *RXTE X-Ray Observations*

XTE J1118+480 was intensively monitored in X-rays with the *Rossi X-Ray Timing Explorer* (*RXTE*) from 2005 January 13 to February 26. There are two narrow-field instruments aboard *RXTE*, the Proportional Counter Array (PCA) and the High-Energy X-Ray Timing Experiment (HEXTE). Due to the faintness of the source throughout the outburst, only the more sensitive PCA produced useful data. For this work, we only used data taken in the Standard1b mode, which provides a time resolution of 1/8 s and covers a nominal energy range of 2–60 keV. The PCA data were reduced with FTOOLS (version 5.2), which was distributed as a part of the software suite HEASOFT.[9] Briefly, for each observation, we simulated background events with the appropriate background model. The data were then filtered in the usual manner,[10] which resulted in a list of good time intervals (GTIs). Using the GTIs, we proceeded to extract a light curve from the data and background files, respectively. The background-subtracted light curve was rebinned to 1/4 s for cross-correlation analysis. The only X-ray data used in this work are those with an overlap with optical data.

[9] See http://heasarc.gsfc.nasa.gov/docs/software/lheasoft.

[10] See the online *RXTE* Cook Book at http://heasarc.gsfc.nasa.gov/docs/xte/recipes/cook_book.html.

3. ORBITAL LIGHT CURVES

The best data for searching for an orbital or superhump modulation is the SARA photometry, as this has the longest periods of coverage, and longer exposures suffer less scatter due to the large-amplitude flickering present. A modulation on a period of about 4 hr is seen on both nights at about the same full amplitude of ~2.0% (Fig. 1). A period search including both nights of data finds several closely spaced aliases. One of them is at 0.17036(24) days or 1.0025(14) $P_{\rm orb}$ (assuming the period of Zurita et al. 2002). This is consistent with previously reported superhump periods, e.g., 0.170529(6) days (Uemura et al. 2002), but does not securely rule out an orbital modulation. Aliases at 1.09 $P_{\rm orb}$ and 1.20 $P_{\rm orb}$ are statistically slightly preferred to that at the superhump period. The similarity to previous observations points to the solution closest to the orbital period as the correct one, however, as this is consistent with the finding of Chou et al. (2005) of a very weak (0.02 mag) modulation close to the orbital (or superhump) period after January 18. In contrast, the superhump identified by Uemura et al. (2002) throughout the 2000 outburst exhibited a persistent modulation with an average full amplitude of about 7%, so our observations and those of Chou et al. (2005) indicate a weaker superhump in this outburst.

Where we have observations of at least one binary orbit in other data, we examined the light curves for evidence of a similar superhump modulation. These other light curves are less well suited, as rapid variability is not averaged out. We find no evidence of any such modulations in either the optical or IR data. The optical light curve from January 16 places a 2 σ (95%) upper limit on the full amplitude of a sinusoidal modulation at the orbital period (for any phasing) of 3.5% of the flux. We attempted to analyze the IR light curves in the same way and, while no consistent modulation was apparent, the formal limits derived were much weaker. This is a consequence of the larger intrinsic variance due to flaring, and the much lower duty cycle reducing the ability to average over many flares. Upper limits obtained were 7%–16% in J, 12%–19% in H, and 17%–24% in K_s.

4. POWER DENSITY SPECTRA

Our best time sampling is in the fast optical photometry from 2005 January 13, 1 s time resolution with negligible dead time. In Figure 2 we show the power spectral density (PSD) of the differential light curve between the target and comparison star.

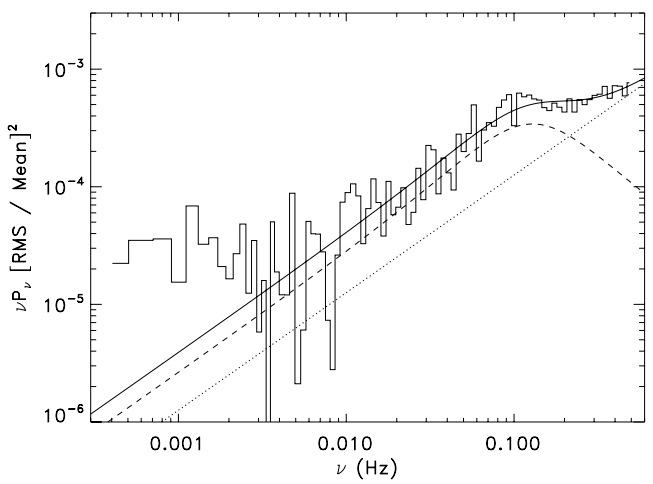

FIG. 2.— Power-spectral density derived from fast photometry on 2005 January 13, in unfiltered white light, showing a single-Lorentzian component (*dashed line*), the fitted white-noise level (*dotted line*), and the combined fit (*solid line*). Fits only used data above 0.01 Hz, where source variability is dominant.

Examining the PSDs of each star individually, the target exhibits excess power above about 0.01 Hz, even though it is brighter, while below that both stars have the same power, likely due to transparency variations and/or aperture losses. We are therefore confident that the power in the differential PSD above 0.01 Hz should be due to real variations in the target, apart from white noise, which dominates at the very highest frequencies. We have shown the PSD in the now common νP_ν form and show a fit comprising a single Lorentzian component plus white noise (Belloni et al. 2002). The Lorentzian frequency parameters are a characteristic frequency $\nu_{\max} = 0.13$ Hz and central frequency $\nu_0 = 0.065$ Hz; $\nu_{\max}$ corresponds to the peak in νP_ν and is given by $\nu_{\max} = \left(\nu_0^2 + \Delta^2\right)^{1/2}$, where Δ is the half-width at half-maximum of the Lorentzian. The difference from a zero-centered Lorentzian is small, corresponding to a low coherence, $Q = 0.11$. The PSD derived is thus very similar to those seen during the 2000 outburst, although the break frequency, $\nu_{\max}$, is higher than seen then, when it evolved from about 0.03–0.08 Hz (Hynes et al. 2003).

If the PSD did not change substantially between 2005 January 13 and 19 and is similar in the IR and optical, then this gives us information about how well the IR observations resolve variability. The single fitted Lorentzian component has 90% of its power on timescales 0.9–70 s. Thus, most of the variability ($\gtrsim$90%) is on timescales shorter than the $\sim$50 s sampling time, and hence consecutive points are effectively independent. On the other hand, most of the variability is on timescales longer than the IR exposure time; hence the IR observations should not smooth out much of the variability and should sample most of the dynamic range expected.

5. X-RAY OPTICAL CORRELATIONS

A small amount of overlapping X-ray and optical/IR data were obtained. The poor duty cycle of the IR data resulted in only a handful of points and no measurable correlation. A correlation was seen between X-ray and optical variability, based on a total of approximately 11 minutes of overlap with McDonald 2.7 m White Guider photometry. Figure 3 shows the cross-correlation function (CCF) from 2005 January 16. Since the optical exposure times were quite long, this was calculated by averaging the X-ray data over the duration of each optical exposure (after applying the lag). The CCF is not of high quality, and the 3 s time resolution (set by the exposure duration, not the cycle time) limits the precision of the information obtained, but a lagged correlation is clearly present. The centroid and width of the CCF peak are comparable to those seen by Kanbach et al. (2001) during the 2000 outburst, although the lower time resolution of our data do not permit a detailed comparison.

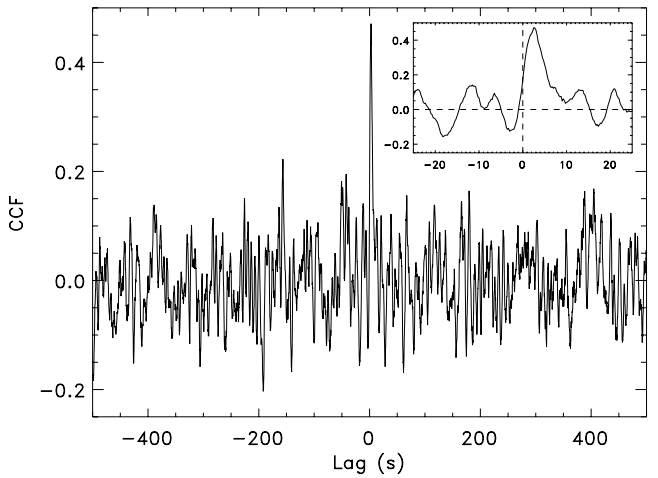

FIG. 3.—Cross-correlation function between X-ray and 3 s time resolution optical data from January 16. *Inset*: Expanded view of the peak.

6. THE SPECTRAL ENERGY DISTRIBUTION (SED) OF THE IR NOISE

6.1. *Observational Results*

Since J, H, and K_s are observed simultaneously, each image set provides an instantaneous IR SED. Comparison of them allows us to study the SED of the IR variability, even though we do not resolve individual flares in time. As a relatively large number of such image sets was obtained, we applied quite cautious standards in filtering the data. We excluded all sets of images in which (1) the seeing was greater than 1.″7, (2) the sky subtraction in any band was poor, (3) the J sky was high in twilight, (4) conditions did not appear photometric (as measured by the comparison star), or (5) the target coincided with either a hot pixel or an α-particle hit on the detector. Table 2 lists the number of good image sets remaining after applying these cuts to the sample. In Figure 4 we show examples of $J - H$ and $H - K_s$ flux relations for the first and last nights and all nights with 2 s data combined. The cuts applied do appear to have cleanly removed bad data, leaving well-defined correlations. We also show equivalent points for the comparison star. For the latter each night's fluxes have been divided by the median, so this is a measure of the scatter in fluxes within a night. If systematic effects, for example, variable extinction due to cirrus, were affecting our data, then we would expect the comparison star to exhibit correlated errors in different bands. No such correlation is seen, suggesting that the uncertainties are dominated by random statistical noise. The uncertainties in the comparison (which should be larger than those in the brighter target) are clearly much smaller than the observed variations in the target fluxes. The scatter about the correlation line in the target may be statistical, however.

We performed the same analyses on the data from the third night, for which 1 s exposures were taken, to test whether shorter exposures sampled a larger dynamic range of the variability. This does not obviously appear to be the case, which is consistent with most of the power being at lower frequencies (§ 4). Since these data are noticeably noisier than the other nights, we have not shown them in the plots. The overall distribution of fluxes is intermediate between those of the preceding and the following nights, with no obvious differences other than the higher noise level.

Figure 4 shows clear and repeatable correlations between bandpasses. Not only do the fluxes within a given night trace out a well-defined relationship, but successive nights appear to follow approximately the same correlation, with the overall brightness declining along the same line as the variations within a night. This points to a very consistent IR behavior and SED, and probably a single spectral component is dominant. The consistency, coupled with the linearity over a factor of 2 in flux, suggests that the shape of the IR SED is not changing, only the overall flux level.

We can use the correlations to estimate the shape of the variable component of the IR SED, since the slope of the correlation, for example, dF_K/dF_H, is a measure of the slope of the SED variations between H and K. This measure is independent of any nonvarying zero point, making this potentially a more sensitive discriminant between models than the overall SED, which may be a sum of several spectral components (e.g., Markoff et al. 2001; Yuan et al. 2005).

6.2. *Power-Law Models*

The simplest model for the IR SED is a power law. We also tested broken power laws (i.e., allowing a different slope for $J - H$

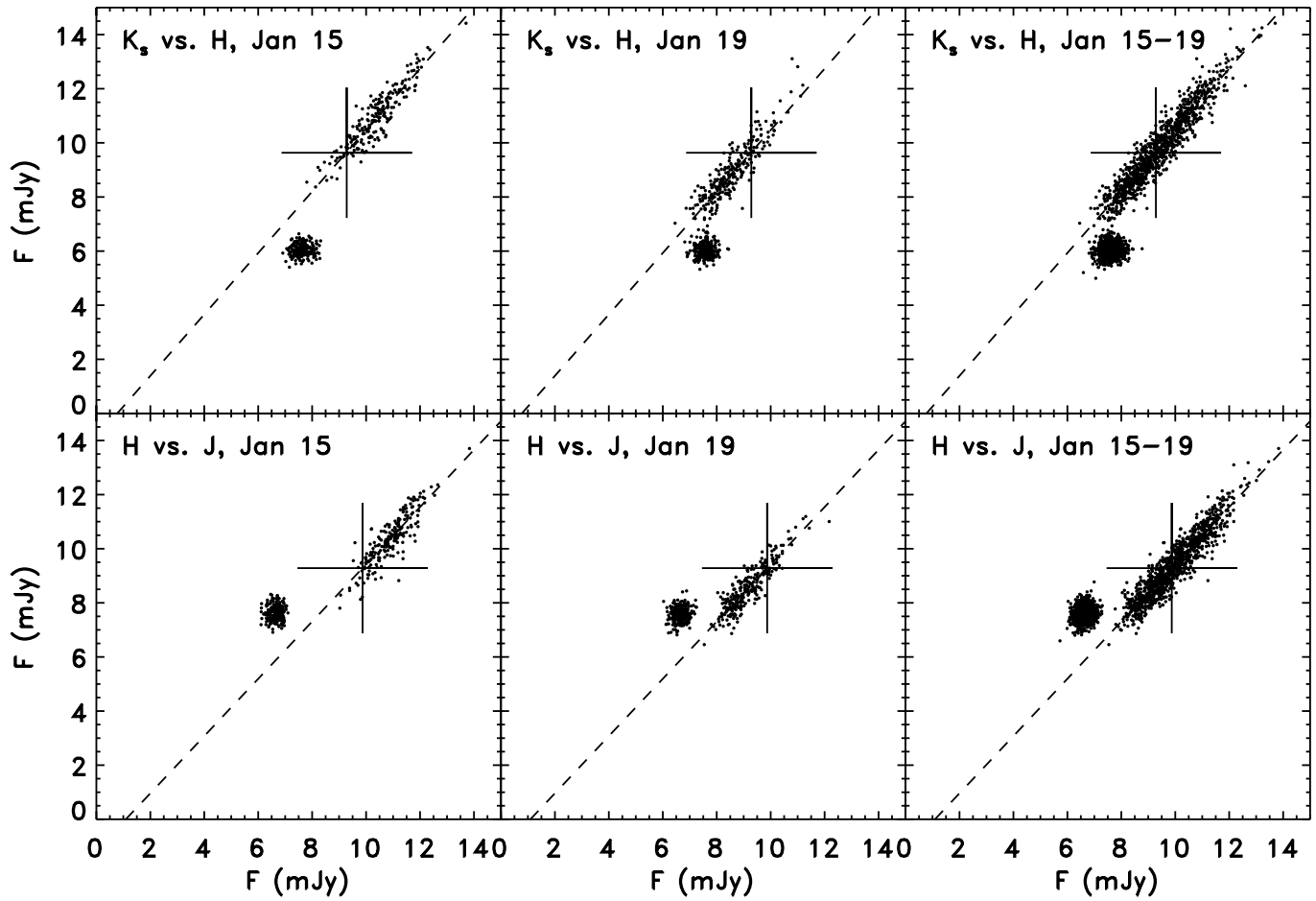

FIG. 4.—J vs. H and H vs. K_s fluxes for the first night, the last night, and all nights with 2 s data combined. Two clusters of points are present on each plot. The diagonally dispersed ones are XTE J1118+480; the circular clump is the comparison star. The dashed lines all show the same linear fit to the combined data set (for that color), to provide a point of reference in comparing the first and last night. The cross indicates the run-averaged fluxes as a point of reference. The joint fit shown here is also only intended as a reference point, and all analyses used night-by-night fits.

and $H - K_s$), but did not find a convincing pattern (see Table 3). There is a tendency for the $J - H$ slope to become flatter and for the $H - K_s$ one to begin steeper (corresponding to a concave spectrum), but suspiciously the $J - K_s$ slope stays approximately constant and tracks a single–power-law fit to the full JHK_s data sets. This suggests either that the H data are less reliable or that adjacent bands simply do not provide adequate leverage in wavelength. We therefore see no compelling reason to believe that the spectral slope really changes across the near-IR and proceed to fit a single power law to the combined JHK_s data for each night; the following discussion relates to this joint fit. Note that given three points in wavelength, such a broken power-law model should be sufficient to completely describe the wavelength dependence, and this test can also be thought of as testing whether there is a significant and repeatable curvature of the spectrum.

Free parameters in the unbroken power-law model are the assumed zero-point fluxes in each band (we adopt the mean), the normalization of the power law for each image set, and the power-law slope. For n JHK image sets there are thus $n + 4$ free parameters and $2n - 4$ degrees of freedom (dof's). The resulting fits typically yielded a χ^2 value of about 2 per dof, assuming only statistical errors. It is likely that the errors are underestimated in this way, as we did not perform differential photometry, and hence aperture losses and small transparency variations could contribute. To approximately correct for this, we adopt the expedient of rescaling the uncertainties (by a factor of about $\sqrt{2}$) to yield a minimum χ^2 of 1 per degree of freedom. We then estimate the single-parameter uncertainty in the slope, α (defined such that $F_\nu \propto \nu^\alpha$), using the region encompassed by $\Delta\chi^2 = 1$. Our derived slopes are given in Table 3, and we also derive a weighted mean of the slopes of

TABLE 3
POWER-LAW FIT PARAMETERS

Date	α_{JH}	α_{HK}	α_{JK}	α_{JHK}	χ^2/dof[a]
Jan 15	-0.75 ± 0.12	-0.73 ± 0.11	-0.78 ± 0.07	-0.77 ± 0.06	1.890
Jan 16	-0.90 ± 0.08	-0.78 ± 0.09	-0.85 ± 0.04	-0.83 ± 0.04	1.822
Jan 17	-0.30 ± 0.16	-1.04 ± 0.15	-0.67 ± 0.08	-0.70 ± 0.07	1.930
Jan 18	-0.50 ± 0.09	-0.98 ± 0.08	-0.74 ± 0.04	-0.76 ± 0.04	1.996
Jan 19	-0.48 ± 0.07	-1.02 ± 0.08	-0.74 ± 0.06	-0.74 ± 0.05	1.789

[a] χ^2 is for the joint JHK fit.

$\alpha = -0.78$. The four nights are consistent with their weighted mean to within the quoted errors, and there is no overall trend in the values, suggesting a constant spectral index over the period observed.

Given that the statistical uncertainty is small and the night-to-night consistency is good, the dominant error will arise from the systematic uncertainty in absolute calibration. Using our estimate of the absolute calibration uncertainties from § 2.4, we estimate using a Monte Carlo calculation that the random uncertainty in the derived power-law index will be about ± 0.07. This assumes that errors in J, H, and K_s are independent. If they are positively correlated, then the uncertainty in the power-law index will be reduced. Only if there is an anticorrelation between J and K_s errors will we have underestimated the uncertainty in the power-law index, and this is unlikely. This calibration uncertainty dominates the other terms so far discussed. The final problem that introduces a systematic bias, rather than a random scatter, is that the variability is redder than a stellar SED. We have treated the photometry as yielding monochromatic fluxes at the bandpass center, but the measurements actually represent weighted averages over the bandpass. In practice this effect is not large, however, so we neglect it. Glass (1999, p. 47) estimates that the corrections to near-IR fluxes to convert them to the monochromatic flux at the bandpass center are only a few percent for power laws of spectral index between -2 and $+2$. We estimate with some simplistic simulations that for our JHK_s photometry, with the spectral slope derived, the resulting error in the spectral slope is likely to be less than 0.01 and much less than other uncertainties. We have therefore not attempted a more rigorous treatment.

In summary, all of our observations are consistent with a single power law of constant slope, $\alpha = -0.78 \pm 0.07$, where the dominant uncertainty is in the absolute calibration of the photometry.

6.3. *Blackbody Models*

A common paradigm for optical variability in X-ray binaries is that it arises in reprocessed X-rays. X-ray irradiation deposits energy at a modest optical depth in the atmosphere of the disk or companion star. This is then thermalized and emerges as optical and ultraviolet flux, which would, simplistically, be expected to have something close to a blackbody SED. This interpretation was rejected based on detailed analysis of the variability during the 2000 outburst (Kanbach et al. 2001; Hynes et al. 2003). Our results further support this, as the variability we see is clearly too red to arise in blackbody emission from the binary. Blackbody fits analagous to those discussed the preceding section yield temperatures $\sim$1500 K, too low for this to be a plausible interpretation.

6.4. *Optically Thin Thermal Models*

Although an optically thick thermal model is not plausible, given the redness of the variability, optically thin thermal emission could still explain the spectral shape, as the free-free emissivity increases with wavelength, resulting in a redder SED than that of a blackbody. Pearson et al. (2005) derived analytic expressions for the time-dependent continuum spectra exhibited during flickering and flaring events. The additional flux was modeled as arising from a region of gas with uniform temperature and Gaussian density profile, expanding with a radial velocity proportional to the distance from the center. Both free-free and bound-free emission mechanisms were considered, and the results of fitting to observations consistently showed that the expansion exhibited isothermal evolution. In the optically thin limit, the observed flux is given by

$$F = \frac{\pi a^2 B}{2d^2}\tau_0 \tag{1}$$

$$= \frac{\pi a^2 B}{2d^2}\left(\frac{\kappa_1 M^2}{\sqrt{2\pi^5}a^5 T^{1/2}}\frac{1-e^{-h\nu/kT}}{\nu^3}\right) \tag{2}$$

$$= e^{-h\nu/kT}\left(\frac{h\kappa_1 M^2}{\sqrt{2\pi^3}c^2 d^2 a^3 T^{1/2}}\right) \tag{3}$$

$$\equiv \alpha_\nu f, \tag{4}$$

where a is the length scale of the Gaussian ($=\sqrt{2}\,\sigma$), B is the Planck function, τ_0 is the optical depth through the center of the expansion, d is the distance to the object, T is the temperature of the region, and M is its mass. The term κ_1 is a constant that depends on the composition and the emission mechanism (i.e., whether free-free or bound-free), and α_ν and f encapsulate a number of terms from equation (3), while separating the wavelength dependence into α_ν alone.

Since the quantities contributing to f are fixed for a given observation of a particular flicker, the ratio of flux in each wave band is given by the ratio of the values for α_ν. Experience suggests that not only is T constant for a particular event, but is also fairly consistent between flickers. The linear relationship between fluxes in the different wave bands can thus be understood as a reflection of the linear relationship between the flux and the parameter f.

For each data triple, consisting of the flux in the JHK_s wave bands, we can derive a best-estimate instantaneous value for f. We can then fit a straight line to $F(f)$ in each wave band simultaneously and extract a best-fitting value for α_J (or equivalently α_H or α_K), which, in turn, is a simple function of T. In practice, rather than a single parameter, we also have to allow for a zero-point offset in the flux in each wave band to account for constant or slowly varying contributions from other parts of the system. The derived values of T are given in Table 4 and have χ^2/ν similar to the power-law fits in § 6.2.

TABLE 4

Derived Temperature from the Flickering Occurring on Each Night for an Optically Thin Thermal Model

Date	Temperature (K)	χ^2/ν
Jan 15	11,500	1.888
Jan 16	10,600	1.819
Jan 17	12,800	1.940
Jan 18	11,700	2.008
Jan 19	12,000	1.797

As a consistency check, we can insert the condition that material be optically thin ($\tau_0 < 1$) into equation (1). This gives us

$$a_{\rm thin} > \sqrt{\frac{2d^2F}{\pi B}} \tag{5}$$

$$\gtrsim 3\times 10^9 \text{ m}, \tag{6}$$

using $d = 1.8$ kpc, $T \sim 12{,}000$ K, and $F_K \sim 20$ mJy. Unfortunately then, while the thermal models do manage to reproduce the data as well as a power law, they require an emitting region comparable in size to the entire binary ($a \sim 2\times 10^9$ m). It is hard

to envisage how this could arise from material within the primary's Roche lobe. This difficulty suggests that, despite the attractiveness of the fit, the emission mechanism in this case is not thermal in origin, and hence that our original power-law fits are probably most meaningful.

7. DISCUSSION

The properties of the variability we observe are very similar to those seen during the 2000 outburst, for example, the prompt correlation with X-rays, the shape of the PSD, and the increasing variability at longer wavelengths. Both Kanbach et al. (2001) and Hynes et al. (2003) concluded that synchrotron emission was the most likely origin of the variability. Our multicolor observations provide strong support for this interpretation. We have argued that a thermal model, whether optically thick or thin, cannot adequately explain the combination of spectral shape, luminosity, and variability timescales observed. The inferred IR spectral slope, $\alpha \simeq -0.78$, is, on the other hand, quite appropriate for optically thin synchrotron emission.

In the context of the jet model for the broadband SED of XTE J1118+480 presented by Markoff et al. (2001), this implies that the IR variability, and probably also the optical and some UV, originate from the "optically thin postshock jet" component. This may indicate a difference from the models of Markoff et al. (2001) in which the near-IR exhibits a flat spectrum, as this implies that the break between optically thin and partially self-absorbed synchrotron emission occurs at longer wavelengths than the near-IR. The slope we derive, however, $\alpha \simeq -0.78$, appears in good agreement with these models. Our observations therefore provide new tests of these models, allowing the optically thin jet emission to be isolated from the contamination by the disk.

Yuan et al. (2005) consider a coupled accretion-jet model. In this model, the IR emission is mostly due to radiation from the jets, although the contribution from hot accretion flows might not be negligible. The jet contribution is associated with synchrotron emission from electrons that are accelerated by internal shocks in the jets. The spectral distribution of the electrons is assumed to be of power-law shape, $N(E) \propto E^{-p}$ for $E_{\min} \leq E \leq E_{\max}$, where $p = 2.24$. For optically thin synchrotron emission one then expects that the spectrum of the radiation is also of power-law shape, for the most part, with a spectral slope $\alpha = (1 - p)/2 = -0.62$, which is already rather close to that which we observe. Moreover, for XTE J1118+480, the IR emission may be associated with electrons near $E_{\max}$, so its spectrum deviates from the power law and is steeper (Yuan et al. 2005).

8. CONCLUSIONS

We have performed optical, IR, and X-ray observations of rapid variability in XTE J1118+480 during its 2005 outburst. Many characteristics are similar to the 2000 outburst, although there are a few key differences. Superhumps, if present, are weaker than in 2000. The variability also seems concentrated to higher frequencies. Our major novel result is simultaneous J, H, K_s photometry, allowing us to isolate the SED of the IR variability. We find this is red and can be well fitted by a power law, $F_\nu \propto \nu^\alpha$, where $\alpha = -0.78 \pm 0.07$. This result is consistent with optically thin synchrotron emission, but hard to explain with thermal emission. We consider this strong evidence in favor of the interpretation of the variability as arising in synchrotron emission, most likely from a jet. Unlike attempts to model the average SED (e.g., Markoff et al. 2001; Yuan et al. 2005), the variability isolates the synchrotron emission from the disk emission, allowing us to measure the slope of the optically thin component directly and show that the spectral break to self-absorbed emission must occur at longer wavelengths than the near-IR, at least at the time our observations were made.

We are grateful to Michael Merrill for technical assistance with SQIID and John Robertson for assistance with the SARA observations. W. C. acknowledges support from NASA grant NNG 04GI54G. This publication makes use of data products from the Two Micron All Sky Survey, which is a joint project of the University of Massachusetts and the Infrared Processing and Analysis Center, California Institute of Technology, funded by the National Aeronautics and Space Administration and the National Science Foundation. This work has made use of the NASA Astrophysics Data System Abstract Service.

REFERENCES

Belloni, T., Psaltis, D., & van der Klis, M. 2002, ApJ, 572, 392
Carpenter, J. M. 2001, AJ, 121, 2851
Chaty, S., Haswell, C. A., Malzac, J., Hynes, R. I., Shrader, C. R., & Cui, W. 2003, MNRAS, 346, 689
Chou, Y., Chen, A., Chiang, P. S., Chen, A. C., Lin, Z. Y., & Chung, Y. 2005, ATel, 399
Cutri, R. M., et al. 2003, The 2MASS All-Sky Catalog of Point Sources (Pasadena: IPAC)
Glass, I. S. 1999, Handbook of Infrared Astronomy (Cambridge: Cambridge Univ. Press)
Hunt, L. K., Mannucci, F., Testi, L., Migliorini, S., Stanga, R. M., Baffa, C., Lisi, F., & Vanzi, L. 1998, AJ, 115, 2594
Hynes, R. I., Mauche, C. W., Haswell, C. A., Shrader, C. R., Cui, W., & Chaty, S. 2000, ApJ, 539, L37
Hynes, R. I., et al. 2003, MNRAS, 345, 292
Kanbach, G., Straubmeier, C., Spruit, H. C., & Belloni, T. 2001, Nature, 414, 180
Markoff, S., Falcke, H., & Fender, R. 2001, A&A, 372, L25
McClintock, J. E., et al. 2001, ApJ, 555, 477
Nather, R. E., & Mukadam, A. S. 2004, ApJ, 605, 846
Pearson, K. J., Horne, K., & Skidmore, W. 2005, ApJ, 619, 999
Pooley, G. G. 2005, ATel, 385
Remillard, R., Garcia, M., Torres, M. A. P., & Steeghs, D. 2005, ATel, 384
Rupen, M. P., Dhawan, V., & Mioduszewski, A. J. 2005, ATel, 387
Uemura, M., et al. 2002, PASJ, 54, 285
Yuan, F., Cui, W., & Narayan, R. 2005, ApJ, 620, 905
Zurita, C., et al. 2002, MNRAS, 333, 791
———. 2005a, ATel, 383
———. 2005b, ATel, 428
———. 2006, ApJ, 644, 432